Brain network motifs are markers of loss and recovery of consciousness

Author information: Catherine Duclos, Ph.D.*,[1,2] Yacine Mahdid, B.Sc.*,[1,2] Danielle Nadin, B.Sc.,[1,2] Vijay Tarnal, M.D.,[4] Paul Picton, M.D.,[4] Giancarlo Vanini, M.D.,[4] Goodarz Golmirzaie, M.D.,[4] Ellen Janke, M.D.,[4] Michael S. Avidan, M.B.B.Ch.,[5] Max B. Kelz, M.D., Ph.D.,[6] George A. Mashour, M.D., Ph.D.,[4] Stefanie Blain-Moraes, Ph.D.[1,2]

* These authors contributed equally to the work

1. School of Physical and Occupational Therapy, McGill University, Montreal, Canada
2. Montreal General Hospital, McGill University Health Centre, Montreal, Canada
3. Integrated Program in Neuroscience, McGill University, Montreal, Canada
4. Center for Consciousness Science and Department of Anesthesiology, University of Michigan Medical School, Ann Arbor, MI, USA
5. Department of Anesthesiology, Washington University School of Medicine, St. Louis, MO, USA
6. Department of Anesthesiology, Perelman School of Medicine, University of Pennsylvania, Philadelphia, PA, USA

Corresponding Author: Stefanie Blain-Moraes, Ph.D. Montreal General Hospital, Room L11-132, 1650 Cedar Ave, L11-132 Montréal, Québec**,** H3G 1A4 Canada**.** Tel: 514-398-1325 stefanie.blain-moraes@mcgill.ca

Abbreviated Title (Running Head): Network motifs are markers of consciousness

Abstract

Motifs are patterns of inter-connections between nodes of a network, and have been investigated as building blocks of directed networks. This study explored the re-organization of 3-node motifs during loss and recovery of consciousness. Nine healthy subjects underwent a 3-hour anesthetic protocol while 128-channel electroencephalography (EEG) was recorded. In the alpha (8–13 Hz) band, five-minute epochs of EEG were extracted for: baseline; induction; unconsciousness; 30-, 10- and 5-minutes pre-recovery of consciousness; 30- and 180-minutes post-recovery of consciousness. We constructed a functional brain network using both the weighted and the directed phase lag index, on which we calculated graph theoretical network properties, and the frequency and topography of 3-node motifs. Three motifs (motifs 1, 2 and 5) were significantly present across participants and epochs, when compared to random networks ($p<0.05$). While graph theoretical properties varied inconsistently across unconscious epochs (p-values<0.05), the topography of motifs 1 and 5 changed significantly between conscious and unconscious states ($p<0.01$). Our results suggest that anesthetic-induced unconsciousness is associated with a topographic re-organization of network motifs. As motif topographic re-organization may precede (motif 1) or accompany (motif 5) the behavioral return of consciousness, motifs could contribute to the understanding of the neural building blocks of consciousness.

Introduction

The field of network neuroscience has yielded powerful insight into the way the brain is structurally and functionally connected. The application of graph theoretical analysis to neuroimaging techniques has provided evidence that the brain has features of a complex small-world network, with functional modules and densely connected hubs [1,2]. The development of quantifiable brain network properties has led to a better understanding of the anatomical and functional architecture that drives various brain states, including anesthetic-induced unconsciousness. Both electroencephalography (EEG) and functional magnetic resonance imaging (fMRI) studies have shown that propofol-, sevoflurane-, and ketamine- induced unconsciousness induce a functional disconnection of anterior and posterior regions of the cortex [3-8], while propofol and sevoflurane also induce an anteriorization of alpha power from the occipital to the frontal cortex [9-11]. Graph theoretical analysis has demonstrated that global and topographic properties of brain networks are altered during anesthetic-induced unconsciousness [12-16]. While these advances have led to a clearer understanding of how anesthetic-induced unconsciousness creates inhospitable conditions for information processing and transfer [17], these measures describe whole-brain network processes rather than region-specific changes in brain functioning. Moreover, they have shown little ability to reveal subtle changes in the level of consciousness during state transitions, such as induction and emergence from anesthetic-induced unconsciousness.

Motifs are patterns of inter-connections between the nodes of complex networks, with a probability of occurrence that is significantly higher than those in randomized networks [18]. As such, functional motifs have been investigated as the basic building blocks of directed networks

[18-19]. The distribution of motifs across a brain network is organized to support information integration and segregation – key properties associated with consciousness [20-22]. Shin *et al.* showed that motif frequency changes across anesthetic induction, maintenance and recovery, and that some motifs are state-specific [23]. Conversely, Kafashan *et al.* showed that sevoflurane-induced unconsciousness disrupts motifs of weaker correlation strength within and between resting-state networks, but preserves motifs with higher correlation strength [24]. These findings suggest that motifs may reflect the underlying process by which anesthesia suppresses long-range functional connectivity and the complexity of sparsely connected brain regions [16,17,25,26]. This analysis technique shows great promise in revealing granular changes in the brain network (i.e. changes in the building blocks of a network, on a nodal level) across states of consciousness and responsiveness. However, the temporal and topographic relationship between motifs and behavioral responsiveness has yet to be established.

This exploratory study tested the hypothesis that loss and recovery of anesthetic-induced unconsciousness causes a re-organization of network motifs. More specifically, we aimed to identify the network motifs that characterize states of consciousness, and to determine the temporal association between network motifs and the behavioral return of consciousness (i.e. responsiveness). Nine healthy adults underwent a controlled, 3-hour anesthetic protocol, during which high-density EEG was acquired. In the alpha frequency band (8–13 Hz) five-minute epochs of EEG were analyzed across the anesthetic protocol, for: baseline; induction; unconsciousness; 30-, 10, and 5- minutes prior to recovery of consciousness; as well as 30- and 180-minutes post-recovery of consciousness (Fig. 1). We hypothesized that different levels of consciousness have a characteristic motif frequency and topography, which can effectively distinguish conscious responsiveness from anesthetic-induced unconsciousness. Given that motifs may constitute the building blocks of functional networks, we hypothesized that motif frequency

and topography would be more strongly associated to states of consciousness than graph theoretical brain network properties ,which are whole-brain network measures. We also hypothesized that the motifs associated with consciousness would recover prior to the return of behavioral responsiveness.

Results

Graph theoretical brain network properties do not consistently distinguish between states of consciousness

We compared graph theoretical brain network properties across eight 5-minute epochs, where half of the epochs represented periods of behavioral responsiveness (i.e. consciousness) and half represented periods of behavioral unresponsiveness (e.g. unconsciousness). Global efficiency was not significantly different from baseline at any time point (Fig. 2A). The clustering coefficient was significantly increased from baseline at 30-, 10-, and 5-minutes pre-recovery of consciousness ($p < 0.01$, Fig. 2B). Changes in binary small-worldness were driven by changes in the clustering coefficient; this metric was therefore also significantly increased from baseline at 30-, 10-, and 5-minutes pre-recovery of consciousness (not plotted due to redundancy). Modularity was significantly increased from baseline at 30-, 10-, and 5-minutes pre-recovery of consciousness ($p < 0.05$, Fig. 2C). None of the metrics distinguished between the baseline and unconsciousness epochs.

The frequency of motifs does not distinguish between states of consciousness

The total frequency of occurrence of the five unidirectional 3-node motifs (Fig. 3) was compared against 100 null networks to assess motif significance. Across all eight epochs, the frequency of motifs 1, 2 and 5 was significantly higher than in null networks, though this

significance varied across epochs and participants (Fig. 4). Motif 1 was significantly present across epochs and participants (alpha: 98.6%), followed by motif 2 (95.8%) and motif 5 (91.7%). As motifs 3 and 4 did not appear significantly more frequently than in null networks, they were removed from subsequent analyses. The frequency of significant motifs (i.e. 1, 2 and 5) was compared across all epochs. There was no significant difference in motif frequency, indicating that the total number of motifs remains consistent across states of conscious wakefulness, anesthetic-induced unconsciousness and the transitions between these states ($p > 0.05$).

Reconfiguration of motif topography marks changes in states of consciousness

On average across all participants, in the alpha band, nodes that participated in motifs 1 and 5 during conscious wakefulness were consolidated into circumscribed brain areas, with motif 1 dominant in central regions (Fig. 5A) and motif 5 dominant in posterior and peripheral regions (Fig. 5C). Nodes that participated in motif 2 were scattered across the brain and did not cluster into a single spatial pattern. The topographic distribution of motif 1 changed significantly from baseline across unconsciousness, 30- and 10-minutes pre-recovery of consciousness) (ANOVA: $p < 0.001$; *Post hoc* t-tests: $p < 0.01$). The topography of motif 1 returned to its baseline state at 5-minutes pre-recovery of consciousness. The topographic distribution of motif 5 changed significantly from baseline during all four unconscious epochs (i.e. unconsciousness, 30-, 10- and 5-minutes pre-recovery of consciousness) (ANOVA: $p < 0.001$; *Post hoc* t-tests: $p < 0.01$). The topographic distribution of motif 2 did not differ significantly from baseline across any epoch. While individual patterns of motif topography varied slightly from this average pattern, topographical reorganization was more visually apparent in individual subjects than on average for 7 of the 9 participants (see Supplementary Material for examples of individual figures). Topographical re-organization in the theta band was similar to that observed in the alpha band,

while there was no clear re-organization in the delta or beta bands (see Supplementary Material for delta, theta, and beta results).

Topographic distribution of source nodes and alpha power

Using the dPLI, we assessed the lead-lag relationships in every motif to identify which nodes were origins of information flow (i.e. "sources"), and which were destinations of information (i.e. "sinks"). This source node analysis was only conducted for motif 1, given that all nodes in motif 5 are both the source and destination of information flow. Source nodes in motif 1 were located predominantly in anterior regions during baseline consciousness, and shifted towards dominance in central regions during unconsciousness, and 30- and 10-minutes pre-recovery of consciousness (Fig. 5B). Sources returned to anterior dominance upon recovery of consciousness.

We investigated the association between the topographic distribution of alpha power and the changes in anterior-posterior dominance observed in motifs across states of consciousness. Alpha power was consolidated in posterior regions during baseline, 30- and 180-minutes post-recovery of consciousness (Fig. 5D). An increase in frontal alpha power is visually apparent during induction, unconsciousness, 30-, 10- and 5-minutes pre-recovery of consciousness. There was a weak positive correlation between alpha power, and the frequency of motif 1 ($R = 0.26$) and motif 5 ($R = 0.22$).

Discussion

We investigated the motif patterns in human directed functional brain networks to identify statistically significant motifs associated with states of consciousness, and to reveal the temporal changes in these basic network building blocks across loss and recovery of consciousness. The

directed functional networks were constructed from high-density EEG data recorded from human participants before, during and after anesthetic-induced unconsciousness using a protocol that enabled us to assess consciousness-related transitions in brain networks without the confounds of surgical stress, inflammatory burden or polypharmacy that often accompany anesthesia research. Networks were constructed from four epochs associated with consciousness (i.e. behavioral responsiveness), and four epochs associated with unconsciousness (i.e. behavioral unresponsiveness). Across these networks, three types of 3-node functional motifs were statistically significant, labeled as motifs 1, 2 and 5. These motifs were topographically distributed in distinct patterns that re-organized with changes in levels of consciousness. Nodes participating in motif 1 were predominant in anterior and central regions during conscious wakefulness, and shifted posteriorly during unconscious states, with a significant topographic reorganization during unconsciousness, 30- and 10-minutes pre-recovery of consciousness. The topographic distribution of motif 1 nodes returned to baseline patterns 5-minutes pre-recovery of consciousness, and remained indistinguishable from baseline at all post-recovery of consciousness epochs. Nodes participating in motif 5 were concentrated in posterior brain regions during baseline conscious wakefulness; anterior nodes increased their participation in this motif during all unconscious epochs.

We explored several potential explanations regarding the mechanism driving the re-organization of network motifs across states of consciousness. First, we tested the hypothesis that motif re-organization could be attributed to changes in the global functional brain network during anesthetic-induced unconsciousness. Graph theoretical analysis revealed inconsistent changes of the global network across states of consciousness based on measures of clustering coefficient, binary small-worldness and modularity, and no changes in the global efficiency of the network between conscious and unconscious epochs. While the increased clustering coefficients

and modularity we observed for unconscious brain networks are similar to previous findings [12,27], these characteristics were not consistently increased across the entire period of unconsciousness. Indeed, both clustering coefficients and modularity were not statistically different between baseline and unconsciousness. This suggests that, while whole-brain network measures provide global indications of network functioning, they are not systematically different between conscious and unconscious states, and are thus not a plausible mechanism for changes in motif topographic organization. Second, we investigated the hypothesis that the observed motif re-organization was associated with anterior-posterior shifts in alpha power across states of consciousness. The anteriorization, or "frontal dominance" of alpha power has long been associated with anesthetic-induced unconsciousness [10,11,28,29], and the reorganization of motifs 1 and 5 exhibited a similar anterior-posterior shift in dominance across states of consciousness. However, there was only a weak correlation between alpha power and motif frequency, indicating that the shift in alpha power was not driving the observed shift in motif distribution. Finally, we investigated the hypothesis that changes in motif topography were driven by decreased connectivity strength in the overall brain network. Anesthetic-induced unconsciousness has been associated with a variable decrease in the strength of directed functional connectivity across brain regions [15,30,31], which could potentially cause an associated decrease in motif frequency, and a shift in topographic distribution. However, the total frequency of each motif was not statistically different between any of the 8 epochs or across states of consciousness (conscious vs. unconscious), eliminating this as a plausible explanation. Therefore, the redistribution of motifs across states of consciousness reveals granular shifts in brain network organization, which are distinct from macro-level changes in overall network structure. This highlights the novel role of motifs in describing changes in brain connectivity

across states of consciousness, and suggests that motifs may provide complementary information on the brain network correlates of consciousness.

It is instructive to examine the characteristics of the significant motifs in finer detail. We observed that three classes of 3-node motifs (i.e. ID = 1, 2 and 5) were significantly more likely to be embedded in human brain networks compared to null networks. These three classes of motifs can be divided into two sub-types, according to their structure: chain-like motifs (ID = 1 and 2) and loop-like motifs (ID = 5). In the chain-like motifs, two nodes that are not directly linked are integrated through an intermediate third node. These chain-like motifs have been implicated in the communication between functional modules of the brain, both in humans and macaques [22,32,33]. Other studies have linked hub regions -- which play an important role in the information integration of the brain network -- to the intermediate apex of these chain-like motifs, and suggest that densely inter-connected hubs (the rich club) form a stable synchronization core through these chain-like motifs [34]. Our source-sink analysis of motif 1 provides further evidence to support these findings. The intermediate apex of this motif is a sink connected to two sources. Across most analysis epochs, the sources are anterior-dominant, and the sinks are posterior-dominant, consistent with the posterior location of hubs during conscious states [35]. Furthermore, one analysis epoch recorded during unconsciousness (i.e. 30 minutes pre-recovery of consciousness) demonstrates a reversal in this pattern, consistent with the anteriorization of hub location observed during anesthetic-induced unconsciousness. The results of our study are thus consistent the growing body of evidence that suggests that chain-like motifs largely contribute to the information integration within the whole-brain network.

Importantly, the topographic re-organization of network motifs may precede or accompany the recovery of consciousness in a motif-specific manner. While spatially complementary, the temporal patterns of topographic re-organization differ between motifs 1 and

5. Indeed, the patterns of motif 5 actively re-organized during unconsciousness and did not return, on average, until participants regained consciousness. Conversely, the patterns of motif 1 re-organized during unconsciousness, but had, on average, returned to their baseline topography by 5 minutes prior to the recovery of consciousness. From this analysis, motif 5 appears to be a marker of the participant's level of consciousness. The temporal characteristics of motif 1 suggest that this network backbone may have potential as an indicator of the imminent return to consciousness, which would be of significant clinical value in monitoring for intraoperative awareness [36], or in assessing pathological unconsciousness such as unresponsive wakefulness syndrome and minimally conscious state [37].

The results of this study must be interpreted in light of several limitations. First, this was a small study of young healthy volunteers, and the patterns of motif distributions observed herein may not generalize to surgical patients of varying ages and comorbidities, nor to brain-injured patients. Secondly, loss and recovery of consciousness were indirectly assessed through behavioral responsiveness. Though we are confident that study participants were deeply anesthetized due to complete unresponsiveness and to the presence of burst suppression and isoelectric EEG in some participants, unresponsiveness is not equivalent to unconsciousness, and awareness may still be present despite unresponsiveness [38]. There have been accounts of intraoperative awareness and no method has yet proven to be completely effective in detecting consciousness (i.e. awareness) during an anesthetic state [39]. Thirdly, the "unconsciousness" epoch represents the first five minutes after isoflurane has been turned off, rather than during isoflurane administration. However, in these 5 minutes immediately after the 3-hour deep sedation, participants were unresponsive, and remained completely unresponsive for over 30 minutes. This was a state of deep unresponsiveness, without the direct effect of isoflurane administration. Fourthly, as our directed functional network was constructed using directed phase

lag index (dPLI), our analysis was limited to motifs with unidirectional connections between nodes. In the class of 3-node motifs, this restricted the scope of our analysis to 5 of the 13 potential 3-node motifs. While the patterns of motif distribution described in this paper remain valid, it is possible that the motifs highlighted herein are in fact a subgraph (i.e. a graph formed by a subset of the vertices of a larger graph) of bidirectional motifs. Constructing the directed functional network with a metric such as symbolic transfer entropy would enable non-complementary measures of bi-directional interactions between nodes, and merits future work [40]. Finally, our interpretation of the topographic distribution of motif 5 as a marker of level of consciousness is limited by the study design, where the first available resting-state epoch post-recovery of consciousness occurs 30 minutes after the return of responsiveness. Analysis of the networks constructed from epochs immediately following recovery of consciousness are warranted to confirm the relationship of this motif distribution to an individual's level of consciousness.

This study provides preliminary evidence that changes in states of consciousness induce a structured re-organization in the topography of functional network motifs. Though motif frequency remains constant under anesthetic-induced unconsciousness, the motif topography associated with conscious wakefulness shifts during unconsciousness and returns either prior to, or in parallel with the recovery of consciousness, in a motif-specific manner. As such, motifs may reveal the neural building blocks of consciousness, and could improve the monitoring, identification and prognostication of consciousness.

Methods

Participants

Nine healthy volunteers (5 men; 24.4 ± 1.0 years old) were recruited at the University of Michigan, as part of the Reconstructing Consciousness and Cognition study (NCT01911195) [41]. A tenth participant was initially recruited but was subsequently excluded from all analyses due to excessive noise artifacts in the EEG. The study was approved by the Institutional Review Board (HUM0071578), and written informed consent was obtained from all participants. As this was an observational study, it was not registered in a clinical trial registry. Participants were included if they were between 20 and 40 years old, had a BMI < 30 kg/m^2, satisfied the criteria for the American Society of Anesthesiologists Physical status I or II [42], had an easily visualized uvula and were able to provide signed informed consent. Participants were excluded if they had physical indication of a difficult airway, family history of problems with anesthesia, obstructive sleep apnea, neuropsychiatric disorders, hypertension, cardiovascular disease, reflux, sleep disorders, postoperative nausea or vomiting, motion sickness, or reactive airway disease. Participants were also excluded for pregnancy, past or current use of psychotropic medications, current tobacco or alcohol use exceeding 2 drinks/day, positive urine toxicology test, allergy to eggs, egg products, or soy.

Anesthetic protocol

For full study methods, please refer to Maier *et al*. [41]. On the day of the study, participants underwent a standard clinical preoperative history and physical examination. The anesthetic protocol took place in an operating room. Standard electrocardiogram, non-invasive blood pressure cuff, pulse oximeter, and capnography were used for constant monitoring during

the protocol. Patients were pre-oxygenated by face mask prior to induction of general anesthesia with a stepwise increasing infusion rate of propofol: 100 mcg/kg/min × 5 minutes increasing to 200 mcg/kg/min × 5 minutes, and then to 300 mcg/kg/min × 5 minutes. During this time, an audio loop command was played every 30 seconds, asking the participant to squeeze their left or right hand twice (randomized order). Loss of consciousness was estimated through loss of responsiveness, which was defined as the first time that a participant failed to respond to two consecutive commands. After 15 minutes of propofol administration, inhalation of 1.3 age-adjusted minimum alveolar concentration (MAC) of isoflurane was started [43]. A laryngeal mask was inserted orally, a nasopharyngeal temperature probe was placed, and the propofol infusion was discontinued. Anesthetized subjects received 1.3 age-adjusted MAC inhaled isoflurane anesthesia for 3 hours. Blood pressure was maintained within 20% of baseline pre-induction values using a phenylephrine infusion or intermittent boluses of ephedrine, as necessary. To prevent post-anesthetic nausea and vomiting, participants received 4 mg of intravenous ondansetron 30 minutes prior to discontinuation of isoflurane.

At the end of the 3 hour anesthetic period, isoflurane was discontinued and the verbal command loops were restarted every 30 seconds. The laryngeal mask was removed when deemed medically safe by the attending anesthesiologists. Recovery of consciousness was estimated through return of responsiveness, which was defined as the earliest instance in which participants correctly responded to two consecutive audio loop commands.

Electroencephalographic acquisition and preprocessing

EEG was acquired using a 128-channel system from Electrical Geodesics, Inc. (Eugene, OR) with all channels referenced to the vertex (Cz). Electrode impedance was maintained below 50 kΩ prior to data collection and data were sampled at 500 Hz. Throughout the experiment, data

were visually monitored by a trained investigator to ensure continued signal integrity. Five-minute epochs of EEG were extracted for the following time points: 1) baseline; 2) induction; 3) unconsciousness; 4) 30 minutes prior to recovery of consciousness; 5) 10 minutes prior to recovery of consciousness; 6) 5 minutes prior to recovery of consciousness; 7) 30 minutes post-recovery of consciousness; and 8) 180 minutes post-recovery of consciousness (Fig. 1). Four of these epochs were associated with a state of consciousness (epochs 1, 2, 7, 8) and four were associated with a state of unconsciousness (epochs 3, 4, 5, 6). EEG data were bandpass filtered between 0.1 and 50 Hz and re-referenced to an average reference. Non-scalp channels were discarded, leaving 99 channels for the subsequent analyses. All epochs and channels with noise or non-physiological artifacts were visually identified and removed. We then band-pass filtered the cleaned EEG data into delta (1–4 Hz), theta (4–8Hz), alpha (8–13Hz), and beta (13–30 Hz) frequency bands. Analysis of the alpha band were presented in the main body of the paper, while analyses of other frequency bands are included in the supplementary material.

Functional Connectivity

To construct a functional brain network from EEG data, we used the weighted phase lag index (wPLI) [44], and the directed phase lag index (dPLI) [45] (Fig. 6), which are robust methods to avoid volume conduction confounds in the data [46].

First, we segmented the cleaned EEG data into delta (1-4 Hz), theta (4–8Hz), alpha (8–13Hz), and beta (13-30 Hz) frequency bands using band-pass filtering methods.

wPLI was calculated using the following formula:

$$wPLI_{ij} = \frac{\left|E\{\mathcal{J}(C_{ij})\}\right|}{E\{\left|\mathcal{J}(C_{ij})\right|\}} = \frac{\left|E\{\left|\mathcal{J}(C_{ij})\right| sgn(\mathcal{J}(C_{ij}))\}\right|}{E\{\left|\mathcal{J}(C_{ij})\right|\}}$$

where $\mathcal{J}(C_{ij})$ is the imaginary part of cross-spectrum C_{ij} between signals i and j [44]. The cross-spectrum C_{ij} is defined as $Z_i Z_{j*}$, where Z_i is the complex value Fourier spectra of the signal i for each frequency, and Z_j* is the complex conjugate of Z_j. C_{ij} can be written as $Re^{i\theta}$, where R is magnitude and θ is the relative phase between signal i and j [44]. A wPLI value of 1 indicates complete phase locking between the two signals (i.e. that the instantaneous phase of one signal is leading the other). Conversely, a wPLI value of 0 indicates no consistent phase-lead or -lag relationship. To know the direction of the phase-lead/phase-lag relationship between channels i and j in the wPLI matrix, we calculated the dPLI)[45]. First, the instantaneous phase of each EEG channel was extracted using a Hilbert transform. The phase difference $\Delta\varphi_t$ between all the channels was then calculated where $\Delta\varphi_t = \varphi_{i,t} - \varphi_{j,t}$, t = 1,2,…,N, where N is the number of samples in one epoch, and i and j include all channels. dPLI was then calculated using the following formula:

$$dPLI_{ij} = \langle H(\Delta\varphi_t) \rangle$$

where H(x) represents the Heaviside step function, where H(x) = 1 if x > 0, H(x) = 0.5 if x = 0 and H(x) = 0 otherwise. Thus, if on average signal i leads signals j, dPLI will be between 0.5 and 1, and if signal j leads signal i, dPLI will be between 0 and 0.5. If there is no phase-lead/phase-lag relationship between signals, dPLI = 0.5.

For both the wPLI and dPLI matrices, we controlled for noise-induced phase relationships using surrogate datasets in which we randomized the phase relationship between two channels, while maintaining their spectral properties. More specifically, using the instantaneous phase for each channel pair i and j, we maintained the phase time series for i and scrambled the time series for j from 0 to x, by swapping it for the time series from x to n, where n is the number of samples in one epoch, and 0 < x < n. Data segments used to generate surrogate wPLI/dPLI matrices were

10 seconds in length, and each was permuted 20 times to generate a distribution of values representing the spurious connectivity. The wPLI and dPLI values of the original, non-shuffled EEG data were compared to this distribution of surrogate data using a Wilcoxon signed rank test and were set to 0 (wPLI) or 0.5 (dPLI) if they did not achieve statistical significance. Statistical significance was set to $p < 0.05$.

Construction and analysis of brain networks

The functional brain network was constructed using the wPLI of all pairwise combinations of electrode channels. We constructed a binary adjacency matrix A_{ij} using a threshold of 35%: if the $wPLI_{ij}$ value of nodes i and j was within the top 35% of all wPLI values, $A_{ij} = 1$; otherwise, $A_{ij} = 0$. This threshold was selected because it was previously shown to be the optimum threshold to avoid an isolated node in the EEG network during baseline [47]. From the binary adjacency matrix, we calculated basic graph theoretical network properties, including global efficiency, clustering coefficient, and modularity (Fig. 6). Global efficiency is the inverse of the average shortest path length ($\frac{1}{L_w}$), where L_W is the average of the shortest path lengths (L_{ij}) between all pairs of nodes in the network [48]. The clustering coefficient, calculated by averaging the clustering coefficients of all individual nodes (C_i), represents the degree to which nodes of a graph tend to cluster together, such that higher values imply networks with highly clustered or regular structures [49]. The modularity of the network represents the strength of division of a network into modules, such that high modularity implies a network with strong within-module connections and weak between-module connections [50]. Modularity was calculated using the Louvain algorithm in the Brain Connectivity Toolbox [51]. Finally, small-world organization is characterized by high levels of clustering and short path lengths, meaning that all nodes of a network are linked through relatively few intermediate steps, though they are only directly

connected to a few, mainly neighboring, nodes [1]. Binary small-worldness is therefore the ratio of the clustering coefficient to the average path length, after both metrics are normalized against random networks [52]. Global efficiency and clustering coefficient were normalized by taking the ratio between the true network metric and the average metrics computed for 10 random binary networks, which were generated by shuffling the empirically-generated network's edges 10 times while preserving the degree distributions [53].

Network motifs

In a directed network, a motif is a subnetwork consisting of N nodes and at least (N-1) edges linking the nodes in a path [18,19]. In this study, we investigated network motifs of N = 3 using a unidirectional network, for which 5 motifs are possible (Fig. 3). Each EEG electrode represented a single node; a 3-node motif therefore represents a specific pattern of interconnection between any three electrodes on the scalp (i.e. motifs are not constrained to connections between neighboring electrodes). While motifs comprised of other numbers of nodes are possible, we restrict the analysis in this paper to N = 3 due to the exponential increase in computational complexity that co-occurs with increasingly higher numbers of nodes.

Prior to computing the network motifs, we normalized the dPLI matrix into a non-symmetrical phase-lead matrix, in order to remove redundant information. Given the nature of the dPLI matrix, a value at position (i,j) is necessarily the opposite of a value at position (j,i). We therefore set any value that was below 0.5 in the dPLI matrix, corresponding to a non-phase-leading value, to 0. The remaining non-zero values were normalized between 0 and 1. This normalized phase-lead matrix was then used to calculate the frequency of participation of each node in each motif [51].

Two levels of surrogate analysis were used to calculate whether the probability of occurrence of motifs is beyond chance (i.e. whether a motif is significantly present). First, we corrected for the surrogate number of motifs calculated at each node as follows: using Brain Connectivity Toolbox [51], we generated 100 null networks that preserved the degree and strength distribution from the normalized phase lead matrix. For each of the 100 null networks, we calculated the mean frequency of each motif, for each node. Second, we corrected for the surrogate number of motifs across each network: for each motif, we calculated the total aggregate frequency of motifs in the network by summing across all nodes. We then calculated a network Z-score per motif against the distribution of the total motifs in the 100 null networks as follows:

$$Z_i = \frac{N_i^{real} - < N_i^{null} >}{std(N_i^{null})}$$

where N_i^{real} is the aggregate frequency of motif i across the network and N_i^{null} is the aggregate motif frequency of the 100 null networks [22]. If Z_i was greater than 1.96, the motif was considered to be significant in the network; if not, it was considered non-significant and set to a frequency of 0.

Topographic configuration of network motifs across states of anesthetic-induced unconsciousness

The distribution of nodes participating in each motif was visualized on a topographic head map, using the *topoplot* function of EEGlab [54]. Changes in the topographic distribution of participating nodes were assessed using cosine similarity on the topographic head maps, defined as:

$$s = \frac{b_i \cdot b_j}{\| b_i \| \| b_j \|}$$

where b_i and b_j are vectors containing motif frequencies for states *i* and *j* [23]. Cosine similarity ranges from -1 to 1, where 1 indicates identical topographic distribution, -1 indicates completely opposite topographic distribution, and 0 indicates orthogonality or decorrelation.

Post hoc **analyses**

Once significant motifs were identified, we conducted two additional analyses to further interpret our results.

Topographic distribution of source nodes within a motif

Using the dPLI, we conducted a source node analysis, in which we assessed the lead-lag relationships in every motif to identify which nodes were origins of information flow (i.e. "sources"), and which were destinations of information (i.e. "sinks"). Nodes that were phase-leading other nodes within a motif on their phase relationship were considered sources. Across the total frequency of participation of each node in a given motif, the total number of times that the node behaved as a source was calculated. To assess the topographic distribution of sources within the network, the source total for each node was normalized by computing its Z-score relative to all other node source totals in a given network. These Z-scores were then plotted on a topographic map to visualize the relative distribution of sources within the network.

Topographic distribution of alpha power

We investigated the topographic distribution of alpha power as a possible explanation for the changes in anterior-posterior dominance observed in motifs across states of consciousness. The Pearson correlation between the motif frequency and the raw alpha power ($\mu V/Hz^2$) for each node in the network was calculated. Correlation between alpha power and motif frequency was visualized using a scatterplot, and quantified by computing the Pearson's correlation (R) between

x and y, where x is the motif frequency and y is the power for a given node, across all participants, time points and nodes.

Statistical analyses

The total number of motifs (i.e. sum of motif frequency across all nodes), cosine similarity of motif topographies relative to baseline, and graph theoretical network properties (i.e. global efficiency, clustering coefficient, binary-small worldness and modularity) were compared across epochs using a repeated-measures ANOVA with *post hoc* Bonferroni-corrected t-tests. Cosine similarity values were compared between baseline and all other epochs.

Normality and equal variance assumptions were tested using Shapiro-Wilk and Brown-Forsythe tests, respectively. Two-tailed testing was applied to all statistical tests. Statistical significance was set at $p < 0.05$ for all tests. Statistical analyses were conducted using SigmaStat 4.0.

References

1. Bullmore, E., Sporns, O. Complex brain networks: graph theoretical analysis of structural and functional systems. *Nat rev Neurosci* **10**(3),186-198 (2009).

2. Sporns, O. Graph theory methods: applications in brain networks. *Dialogues Clin Neurosci* **20**(2), 111-121 (2018).

3. Bonhomme, V., *et al*. Resting-state Network-specific Breakdown of Functional Connectivity during Ketamine Alteration of Consciousness in Volunteers. *Anesthesiology* **125**(5), 873-888 (2016).

4. Boveroux, P., *et al*. Breakdown of within- and between-network resting state functional magnetic resonance imaging connectivity during propofol-induced loss of consciousness. *Anesthesiology* **113**(5), 1038-1053 (2010).

5. Jordan, D., *et al*. Simultaneous electroencephalographic and functional magnetic resonance imaging indicate impaired cortical top-down processing in association with anesthetic-induced unconsciousness. *Anesthesiology* **119**(5), 1031-1042 (2013).

6. Lee, U., *et al*. Disruption of frontal-parietal communication by ketamine, propofol, and sevoflurane. *Anesthesiology* **118**(6),1264-1275 (2013).

7. Palanca, B.J., *et al*. Resting-state Functional Magnetic Resonance Imaging Correlates of Sevoflurane-induced Unconsciousness. *Anesthesiology* **123**(2), 346-356 (2015).

8. Ranft, A., *et al*. Neural Correlates of Sevoflurane-induced Unconsciousness Identified by Simultaneous Functional Magnetic Resonance Imaging and Electroencephalography. *Anesthesiology* **125**(5), 861-872 (2016).

9. Akeju, O., *et al*. Disruption of thalamic functional connectivity is a neural correlate of

dexmedetomidine-induced unconsciousness. *eLife* **3**, e04499 (2014).

10. John, E.R., *et al*. Invariant reversible QEEG effects of anesthetics. *Conscious Cogn* **10**(2), 165-183 (2001).

11. Purdon, P.L., *et al*. Electroencephalogram signatures of loss and recovery of consciousness from propofol. *Proc Natl Acad Sci U S A* **110**(12), E1142-E1151 (2013).

12. Blain-Moraes, S., *et al*. Network Efficiency and Posterior Alpha Patterns Are Markers of Recovery from General Anesthesia: A High-Density Electroencephalography Study in Healthy Volunteers. *Front Hum Neurosci* **11**, 328 (2017).

13. Hashmi, J.A., *et al*. Dexmedetomidine Disrupts the Local and Global Efficiencies of Large-scale Brain Networks. *Anesthesiology* **126**(3), 419-430 (2017).

14. Lee, U., Muller, M., Noh, G.J., Choi, B., Mashour, G.A. Dissociable network properties of anesthetic state transitions. *Anesthesiology* **114**(4), 872-881 (2011).

15. Moon, J.Y., Lee, U., Blain-Moraes, S., Mashour, G.A. General relationship of global topology, local dynamics, and directionality in large-scale brain networks. *PLoS Comput Biol* **11**(4), e1004225 (2015).

16. Schroter, M.S., *et al*. Spatiotemporal reconfiguration of large-scale brain functional networks during propofol-induced loss of consciousness. *J Neurosci* **32**(37), 12832-12840 (2012).

17. Lee, U., Mashour, G.A. Role of Network Science in the Study of Anesthetic State Transitions. *Anesthesiology* **129**(5), 1029-1044 (2018).

18. Milo, R. Network motifs: simple building blocks of complex networks. *Scienc*e **298**(5594), 824-827 (2002).

19. Sporns, O., Kotter, R. Motifs in brain networks. *PLoS Biol* **2**(11), e369 (2004).

20. Tononi, G. An information integration theory of consciousness. *BMC Neurosci* **5**:42 (2004).

21. Tononi, G. Integrated information theory of consciousness: an updated account. *Arch Ital Biol*

2012; 150(2-3):56-90.

22. Wei, Y., Liao, X., Yan, C., He, Y., Xia, M. Identifying topological motif patterns of human brain functional networks. *Hum Brain Mapp* **38**(5), 734-2750 (2017).

23. Shin, J., Mashour, G.A., Ku, S., Kim, S., Lee, U. Subgraph "backbone" analysis of dynamic brain networks during consciousness and anesthesia. *PLoS ONE* **8**(8), e70899 (2013).

24. Kafashan, M., Ching, S., Palanca, B.J. Sevoflurane Alters Spatiotemporal Functional Connectivity Motifs That Link Resting-State Networks during Wakefulness. *Front Neural Circuit* **10**, 107 (2016).

25. Barttfeld, P., *et al*. Signature of consciousness in the dynamics of resting-state brain activity. *Proc Natl Acad Sci U S A* **112**(3), 887-892 (2015).

26. Pappas, I.,. Brain network disintegration during sedation is mediated by the complexity of sparsely connected regions. *Neuroimage* **186**, 221-233 (2018).

27. Liang, Z. Information Integration and Mesoscopic Cortical Connectivity during Propofol Anesthesia. *Anesthesiology* **132**(3), 504-524 (2020).

28. Tinker, J.H., Sharbrough, F.W., Michenfelder, J.D. Anterior shift of the dominant EEG rhythm during anesthesia in the Java monkey: correlation with anesthetic potency. *Anesthesiology* **46**(4), 252-259 (1977).

29. Feshchenko, V.A., Veselis, R.A., Reinsel, R.A. Propofol-induced alpha rhythm. *Neuropsychobiology* **50**(3), 257-266 (2004).

30. Blain-Moraes, S., Lee, U., Ku, S., Noh, G., Mashour, G.A. Electroencephalographic effects of ketamine on power, cross-frequency coupling, and connectivity in the alpha bandwidth. *Front Syst Neurosci* **8**,114 (2014).

31. Blain-Moraes, S., *et al*. Neurophysiological correlates of sevoflurane-induced unconsciousness. *Anesthesiology* **122**(2), 307-316 (2015).

32. Gollo, L.L., Breakspear, M. The frustrated brain: from dynamics on motifs to communities and networks. *Philos Trans R Soc Lond B Biol Sci* **369**(1653) (2014).

33. Shen, K., *et al*. Information processing architecture of functionally defined clusters in the macaque cortex. *J Neurosci* **32**(48), 17465-17476 (2012).

34. Gollo, L.L., Zalesky, A., Hutchison, R.M., van den Heuvel, M., Breakspear, M. Dwelling quietly in the rich club: brain network determinants of slow cortical fluctuations. *Philos Trans R Soc Lond B Biol Sci* **370**(1668), (2015).

35. Kim, M., *et al*. Functional and Topological Conditions for Explosive Synchronization Develop in Human Brain Networks with the Onset of Anesthetic-Induced Unconsciousness. *Front Comp Neurosci* **10**,1 (2016).

36. Avidan, M.S., *et al*. Prevention of intraoperative awareness in a high-risk surgical population. *N Engl J Med* **365**(7), 591-600 (2011).

37. Schnakers, C., *et al*. Diagnostic accuracy of the vegetative and minimally conscious state: clinical consensus versus standardized neurobehavioral assessment. *BMC Neurol* **9**,35 (2009).

38. Sanders, R.D., Tononi, G., Laureys, S., Sleigh, J.W. Unresponsiveness not equal unconsciousness. *Anesthesiology* **116**(4), 946-959 (2012).

39. Mashour, G.A., Orser, B.A., Avidan, M.S. Intraoperative awareness: from neurobiology to clinical practice. *Anesthesiology* **114**(5), 1218-1233 (2011).

40. Staniek, M., Lehnertz, K. Symbolic transfer entropy. *Phys Rev Lett* **100**(15), 158101 (2008).

41. Maier, K.L., *et al*. Protocol for the Reconstructing Consciousness and Cognition (ReCCognition) Study. *Front Hum Neurosci* **11**, 284 (2017).

42. Vacanti, C.J., VanHouten, R.J., Hill, R.C. A statistical analysis of the relationship of physical status to postoperative mortality in 68,388 cases. *Anesth Analg* **49**(4), 564-566 (1970).

43. Nickalls, R.W., Mapleson, W.W.. Age-related iso-MAC charts for isoflurane, sevoflurane and desflurane in man. *Br J Anaesth* **91**(2), 170-174 (2003).

44. Vinck, M., Oostenveld, R., van Wingerden, M., Battaglia, F., Pennartz, C.M. An improved index of phase-synchronization for electrophysiological data in the presence of volume-conduction, noise and sample-size bias. *Neuroimage* 55(4),1548-1565 (2011).

45. Stam, C.J., van Straaten, E.C. Go with the flow: use of a directed phase lag index (dPLI) to characterize patterns of phase relations in a large-scale model of brain dynamics. *Neuroimage* **62**(3), 1415-1428 (2012).

46. Stam, C.J., Nolte, G., Daffertshofer A. Phase lag index: assessment of functional connectivity from multi channel EEG and MEG with diminished bias from common sources. *Hum Brain Mapp* **28**(11), 1178-1193 (2007).

47. Kim, H., Hudetz, A.G., Lee, J., Mashour, G.A., Lee, U. Estimating the Integrated Information Measure Phi from High-Density Electroencephalography during States of Consciousness in Humans. *Front Hum Neurosci* **12**, 42 (2018).

48. Latora, V., Marchiori, M. Efficient behavior of small-world networks. *Phys Rev Lett* **87**(19), 198701 (2011).

49. Watts, D.J., Strogatz, S.H. Collective dynamics of 'small-world' networks. *Nature* **393**(6684), 440-442 (1998).

50. Newman, M.E. Modularity and community structure in networks. *Proc Natl Acad Sci U S A* **103**(23), 8577-8582 (2006).

51. Rubinov, M., Sporns, O. Complex network measures of brain connectivity: uses and interpretations. *Neuroimage* **52**(3), 1059-1069 (2010).

52. Humphries, M.D., Gurney, K. Network 'small-world-ness': a quantitative method for determining canonical network equivalence. *PLoS ONE* **3**(4), e0002051 (2008).

53. Maslov, S., Sneppen, K. Specificity and stability in topography of protein networks. *Science* **296**(5569), 910-913 (2002).

54. Delorme, A., Makeig, S. EEGLAB: an open source toolbox for analysis of single-trial EEG dynamics including independent component analysis. *J Neurosci Methods* **134**(1), 9-21 (2004).

Acknowledgements

This work was funded by the James S. McDonnell Foundation, St. Louis, MO (GM, MK and MA); the Canadian Institute for Health Research (FRN 152562, CD; Fredrick Banting and Charles Best Canada Graduate Scholarship – Masters, DN); the Fonds de Recherche du Québec – Nature et technologies (YM); the Fonds de Recherche du Québec – Santé (DN); and the Natural Science and Engineering Research Council of Canada (Discovery Grant RGPIN-2016-03817; SBM).

Competing Interests

The authors declare no competing interests.

Figure Legends

Figure 1. Experimental design and timeline

Timeline of anesthetic protocol and EEG data epochs. Participants received a stepwise increasing infusion rate of propofol for 15 minutes: 100 mcg/kg/min × 5 minutes increasing to 200 mcg/kg/min × 5 minutes, and then to 300 mcg/kg/min × 5 minutes. Participant then received 1.3 age-adjusted minimum alveolar concentration inhaled isoflurane anesthesia for 3 hours. Blue rectangles represent the eight 5-min EEG epochs during which network properties and motifs were calculated: 1) baseline; 2) induction; 3) unconsciousness; 4) 30 min prior to recovery of consciousness; 5) 10 min prior to recovery of consciousness; 6) 5 min prior to recovery of consciousness; 7) 30 min post-recovery of consciousness; and 8) 180 min post-recovery of consciousness.

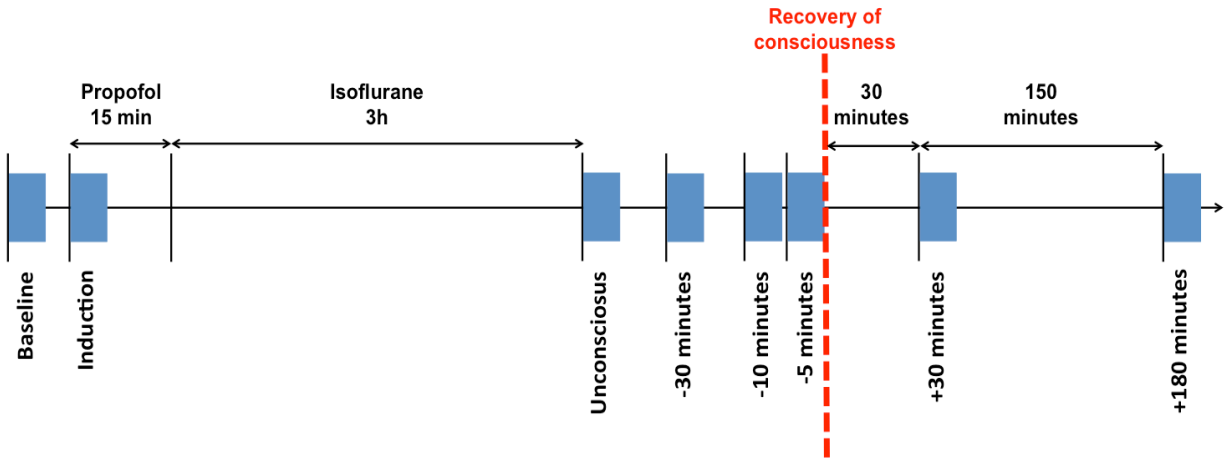

Figure 2. Brain network properties across the experimental period

The functional brain network of each participant was constructed using the wPLI matrix. From this network, we calculated graph theoretical network properties, including global efficiency (A), clustering coefficient (B), binary small-worldness and modularity (C), across the eight analysis epochs. Changes in binary small-worldness were driven by changes in the clustering coefficient; this metric was therefore also significantly increased from baseline at 30-, 10-, and 5-minutes pre-recovery of consciousness (not plotted due to redundancy). Boxes represent the interquartile range, with the lower and upper limit of boxes indicating 1st and 3rd quartiles, respectively. The median is marked by the black horizontal line inside the boxes. The whiskers outside the boxes extend to the lowest and highest observations that are not outliers, while outliers are marked by a cross, and are defined as values greater than ±1.5 times the interquartile range.

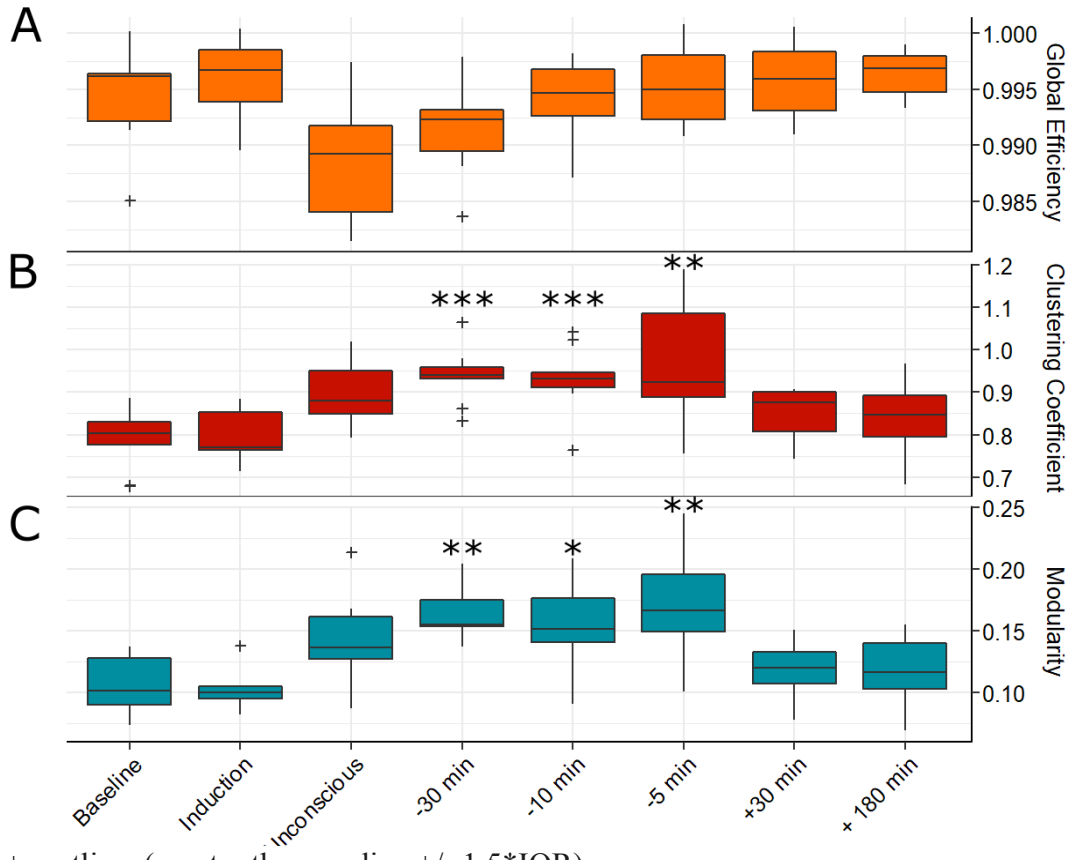

+: outliers (greater than median +/- 1.5*IQR)
*: significantly different from Baseline ($p<0.05$)
**: significantly different from Baseline ($p<0.01$)
***: significantly different from Baseline ($p<0.001$)

Figure 3. Possible 3-node network motifs
A 3-node motif represents a specific pattern of interconnection between three electrodes Five 3-node motifs can exist when unidirectional connections are assessed. These five 3-node motifs are assessed in this study. Dark circles represent nodes (i.e. individual electrodes), while black lines represent the edges linking the nodes. Arrows indicate the direction of phase-lead relationship.

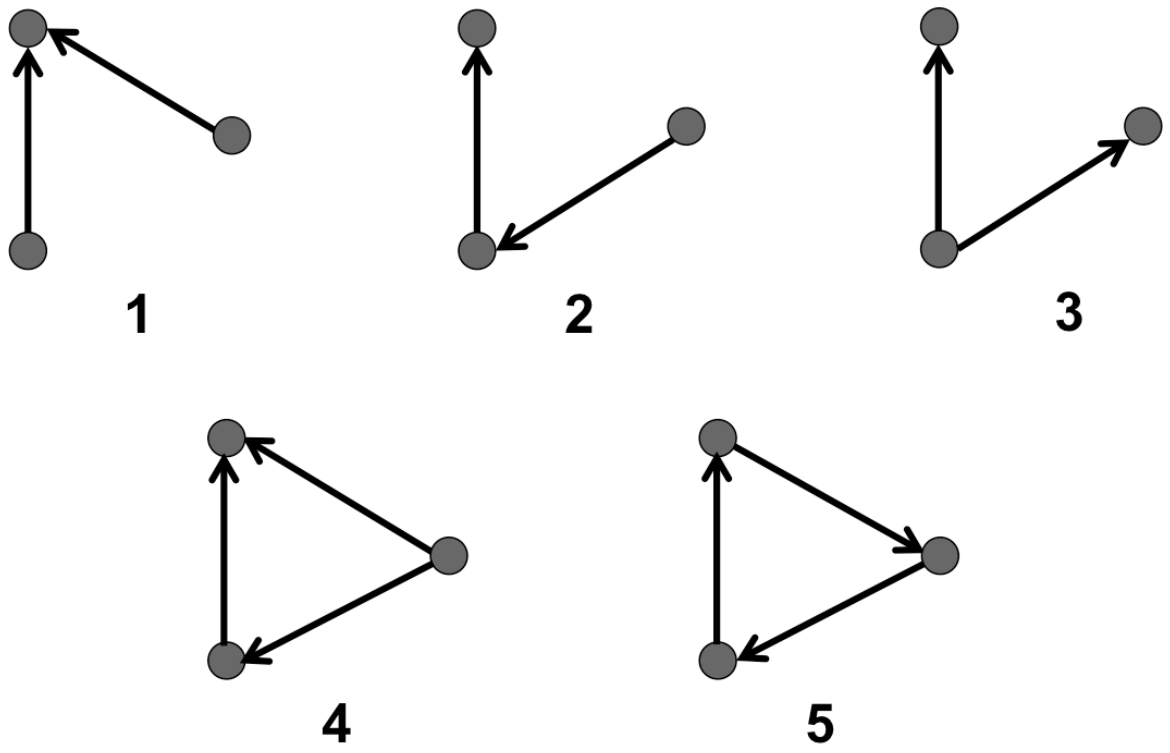

Figure 4. Motif significance

For each motif, the total aggregate frequency of motifs in the network was calculated by summing across all channels. A network Z-score was calculated per motif against the distribution of the total motifs in the 100 null networks. Motifs that were statistically significance per participant and time point are represented by orange (motif 1), purple (motif 2) and green (motif 5) rectangles. Motifs not statistically significant are left grey. Each time point has the potential to be significant in all nine participants, but motif significance varied across time points and participants. Percentages in the right column represent the frequency of motif significance. A frequency of 98.6% in motif significance indicates that this motif was significant throughout all participants and time points, except one participant, at one time point.

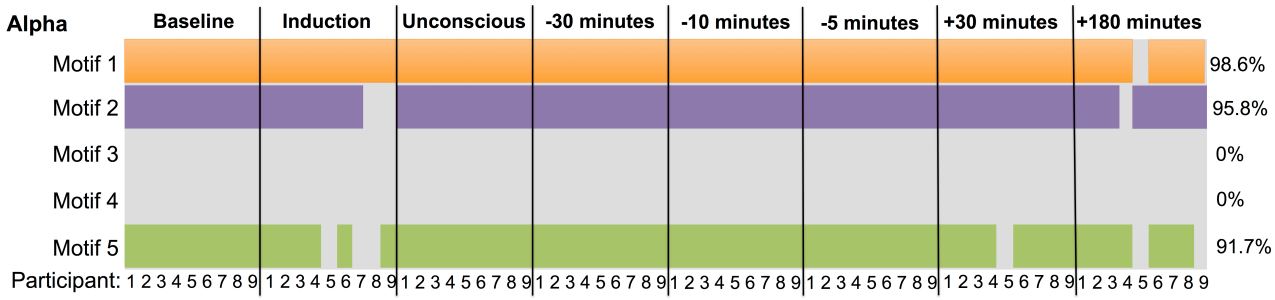

Figure 5. Motif topography across states of consciousness

A and C) Topography of the frequency of participation of nodes in alpha motif 1 (M1) and motif 5 (M5) across the eight analysis epochs. Orange rectangles highlight the epochs that are significantly distinct from Baseline ($p < 0.05$). The colormap represents the Z-score of the normalized frequency of motif participation for each electrode. B) Topographic maps depicting the distribution of nodes acting as sources of information flow (i.e. nodes that have a phase-lead relationship with regards to the other nodes within the motif), in every instance of motif 1 within the EEG network, across the eight time points of the anesthetic protocol. The colormap represents the Z-score of the total source score of each node. D) Alpha power topographic maps across the eight analysis epochs. There is a weak positive correlation between alpha power the frequency of motif 1 (R = 0.26) and motif 5 (R = 0.22). E) Differences in cosine similarity values between Baseline, Unconsciousness, and 180 minutes post-recovery of consciousness. Grey lines depict single participants, while the red line depicts average cosine similarity value across all participants

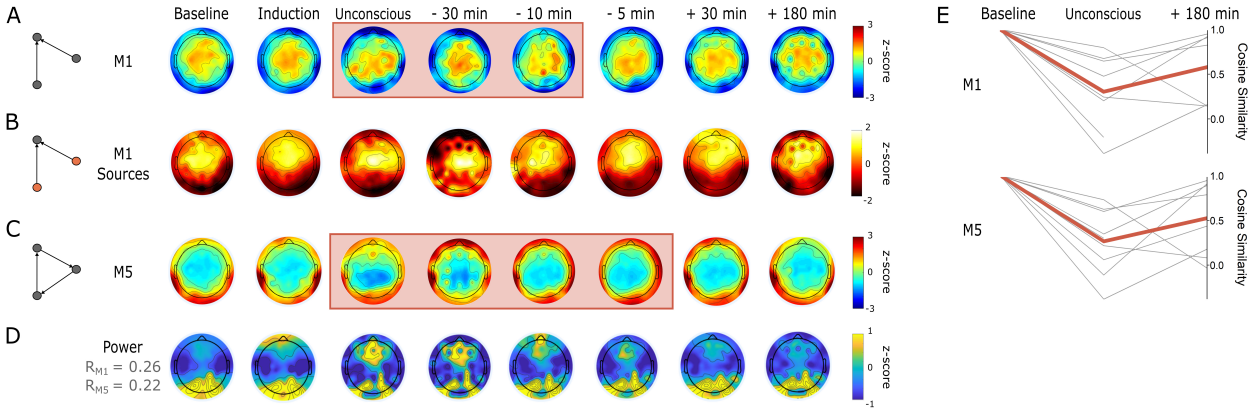

Figure 6. Pipeline for extracting network properties and motifs EEG time series
Each 5-min EEG epoch was used to construct a wPLI and dPLI matrix. Network properties were then calculated based on the wPLI matrix, while the dPLI matrix was used to create a phase-lead matrix, which set all non-phase-leading values to 0 (black), and normalized the remaining non-zero values between 0 and 1. Motifs were then extracted from the phase lead matrix, and their frequency (i.e frequency of participation of a node in each of the possible types of motifs) and topography (i.e. topographic distribution of participating nodes in each motifs) were calculated.

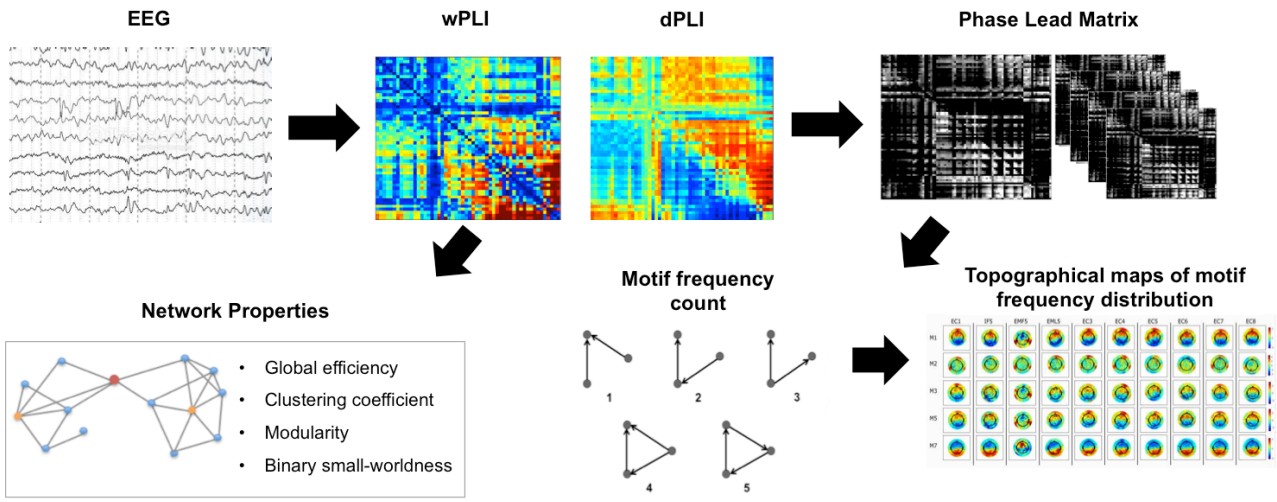

EEG: electroencephalography; wPLI: weighted phase lag index; dPLI: directed phase lag index;